A Submicron Precision Silicon Telescope for Beam Test Purposes

C. Colledani, W. Dulinski, R. Turchetta
LEPSI, IN2P3-CNRS/ULP,
BP20, F-67037, Strasbourg Cedex, France.

F. Djama[1]
CRN, IN2P3-CNRS/ULP,
BP28, F-67037, Strasbourg Cedex, France.

A. Rudge, P. Weilhammer
CERN,
CH-1211 Geneva 23, Switzerland.

Abstract

A precise and compact silicon microstrip detector telescope designed to provide reference information for charged particle tracks has been constructed. First operation results are presented. A signal over noise ratio higher than 100 has been obtained, resulting in a spatial resolution of 1.4 μm per detector, for a readout pitch of 50 μm. At a position in the center of the telescope, a track extrapolation error of 0.7 μm can be obtained for reconstructed tracks.

Submitted to Nuclear Instruments and Methods in Physics Research A.

[1]Corresponding author, e-mail: djama@frcpn11.in2p3.fr

1 Introduction

High precision silicon detectors are commonly used in particle physics. Their ability to reconstruct the decay vertices of short lived particles, by providing precise spatial information close to the primary interaction point, established them among the most essential sub-detectors in collider and fixed target experiments.

Large research and development efforts are being carried out to improve the performances of silicon detectors (double sided sensors [1], pixels [2]), or to develop new kinds of microstrip sensors (diamond [3], gazeous chambers [4], gallium arsenide [5]). An important step in developing a new detector consists of putting it in a high energy beam, in order to measure its characteristics (resolution, efficiency, noise...). It is convenient to have precise information for each track with better resolution than that expected from the tested detector, in order to correctly analyse the performances of the tested detectors.

The silicon telescope described here has been built for this purpose. The mechanics, the readout electronics and the data acquisition system are described in section 2. The performance of the silicon detectors is discussed in section 3. Section 4 is devoted to off-line analysis and section 5 to results.

2 The silicon telescope

2.1 Overview

The telescope has two compact components: a detector frame, and an acquisition frame. Each frame is mounted on a trolley which facilitates its motion.

The detector frame is set up on the beam line. It has three platforms. On the upper one, 4 pairs of silicon detectors are fixed on a precisely machined metal table. In each pair, one detector is measuring the horizontal coordinate (x), while the other gives the vertical one (y). The detectors can be mounted at different positions along the beam axis (z), by means of screws and fixation holes. The maximum distance between the two most external detectors (limited by the table length) is 50 cm. Two small scintillator detectors (1x1 cm^2) are located at each end of the telescope for triggering purposes. The setup is shown in figure 1.

The intermediate platform supports the power supply for readout electronics, while the high and medium voltage sources for PM's (1500 V) and silicon sensors (60 V) are located on the lowest platform.

The second frame is put in the control room and supports the data acquisition system. The CAMAC modules that discriminate the signals from the scintillators are located in the lowest part of the frame. The intermediate part contains the VME

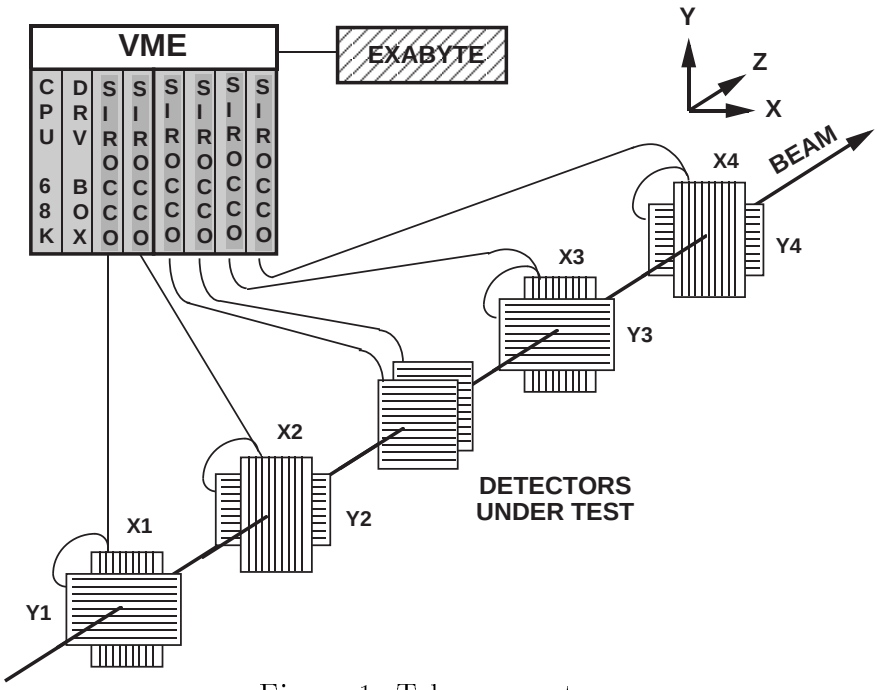

Figure 1: Telescope setup.

Sirocco ADCs, which digitize the analog signals from silicon detectors. The acquisition program runs on an Eurocom CPU card based on a 68030 processor. Data are recorded on Exabyte cassettes and the acquisition is controled from a terminal located on the upper part of the frame.

2.2 The readout electronics

Each silicon sensor (see paragraph 3) is read by 3 low noise VLSI chips, called Viking [6]. The Viking chips have been built in 1.5 μm CMOS technology, and contain 128 channels. Each channel has a charge sensitive preamplifier followed by CR-RC shaper and sample-and-hold circuitry. Each single preamplifier has a power consumption of 1.5 mW. Use of time continuous shaping enhance the acquisition efficiency in the case of trigerred applications, compared with switched capacitors readout architecture.

When a trigger arrives (coincidence of the 2 scintillators of the telescope), the Viking driver box generates the digital clock signals necessary for holding the signal peak value and then starts data readout. Data from each channel are put serially in an output buffer through an on chip multiplexer. The measured noise of the Viking chips, with a peaking time of 2 μs is 135 e^- + 12.3 e^-/pF [6].

2.3 The VME Siroccos

The readout processors Sirocco [7] (SIlicon strip Read Out Camac COntrolers) have been originally developed at CERN to handle the readout of the silicon strip detectors and their associated front-end electronics. They were initially used during our first tests. They were replaced afterwards by VME Siroccos developed at LEPSI especially for tests purposes. They sample and store silicon strip raw data without processing. So all the information is kept for further off-line analysis. The VME data transfer is faster than Camac's (200 ns/cycle against 2 μs/cycle). VME Siroccos enable us to have an homogeneous VME data acquisition system.

The module is a one channel, 10 bit resolution flash ADC running at a 20 MHz maximum conversion frequency. Its input is DC coupled with a dynamic range between -300 and +300 mV, and has a programmable base line through a 12 bit DAC. Converted values are stored in a 4096x11 bit memory, the 12^{th} bit being set on overflow.

The module can run in stand alone mode or in parallel with other modules. In our application, the 6 Siroccos (1 for each pair of reference detectors and 2 for detectors under test) are synchronized by an external clock supplied by the Viking driver.

During the conversion, a status bit is set, and analog data are digitized and stored in the memory on each clock pulse. After 4096 clock cycles or a given programmed value, the Sirocco stops the conversion and the status is cleared. Each address memory corresponds to a silicon strip number. To achieve this, a programmable skip counter allows to keep this relation even if the electronic chips need extra conversion clock cycles to present the data on the serial line.

Finally, the readout of the module is performed by a master CPU through the 24 adresses/16 bits VME slave interface in single data transfer mode.

2.4 The acquisition program

The telescope acquisition program OS9DAS is an adaptation of a portable data acquisition system based on Microdas [8] software, developed for a VME OS9 operating system. This package uses not only all the facilities provided by Microdas, but also OS9 primitives and Real Time Fortran 68K. The kernel is based on a circular buffering scheme with an associated synchronization task, which shares the buffer access between the producer and the consumers. One part of OS9DAS is general and could be implemented in any OS9 system having a Fortran 77 compiler, whereas the second part is user-dependent and could be tailored to a specific hardware configuration.

The main module of OS9DAS is general to any application, and includes setting the run parameters, starting or stopping the run, DAS controle and diagnostic and event words display. It activates also the user front-end modules (Siroccos) and controls the high voltage system.

The producer process starts the transfer of the data from the Siroccos to the buffer memory as soon as it receives an interruption signal from the Viking driver box. For our application, we had 6 Siroccos to read (1280 memory allocation per Sirocco), each VME word (16 bits) transfer takes about 700 ns. The maximum data transfer rate onto the Exabyte tapes was 150 Kbytes/s. Consequently, given the size of one physical event (16 Kbytes), and taking into account a first order real time opimization of the Fortran package, around 80 events could be stored during the beam burst period of 12.5 s. The circular buffer size was set to 1.2 Mbytes.

OS9DAS has many consumer modules which execute several tasks : reading the data, writing them on Exabyte, on-line analysis and results display for a given percentage of acquired events, status display. The buffer manager process takes care of synchronization between the consumers. It has to be activated from all producer and consumers tasks before they can access to the buffer memory.

3 The silicon sensors

The silicon sensors used in the telescope were manufactured by CSEM (Neuchâtel, Switzerland). They are single sided, AC coupled, square shaped (19.2 x 19.2 mm^2), and have a thickness of 360 μm. For such a thickness the most probable charge induced by a minimum ionising particle amounts to 26 000 electrons. The strip pitch is 25 μm while the readout pitch is 50μm (i.e. only one strip out of two is read). There are 384 readout strips on each sensor. Figure 2 shows a schematic top view of a corner of such a silicon sensor. Coupling capacitors are created by insulating the aluminium readout strips from the $p+$ strips by a 200 nm layer of silicon dioxide (SiO_2) deposited at high temperature, and 150 nm of silicon nitride (Si_3N_4). The silicon nitride is etched away between strips.

The sensors are fully depleted at a bias voltage of 60 V. This voltage is applied to the backplane $n+$ implant. The $p+$ implants are connected to a p^+ bias via a punch through structure with a dynamic resistance higher than 100 $M\Omega$ per strip. The average leakage current is less than 0.4 nA per strip. The high value of the polarization resistance and the low value of the leakage current, combined with the low effective capacitance seen by each $p+$ strip ($C_{load} \simeq 4pF$) represent a very low noise contribution from the sensor. If the sensors are operated at a temperature of 20^o C, and if they are bonded to Viking chips, the noise per channel is about 250 electrons, giving a signal over noise ratio higher than 100, as shown in the next section.

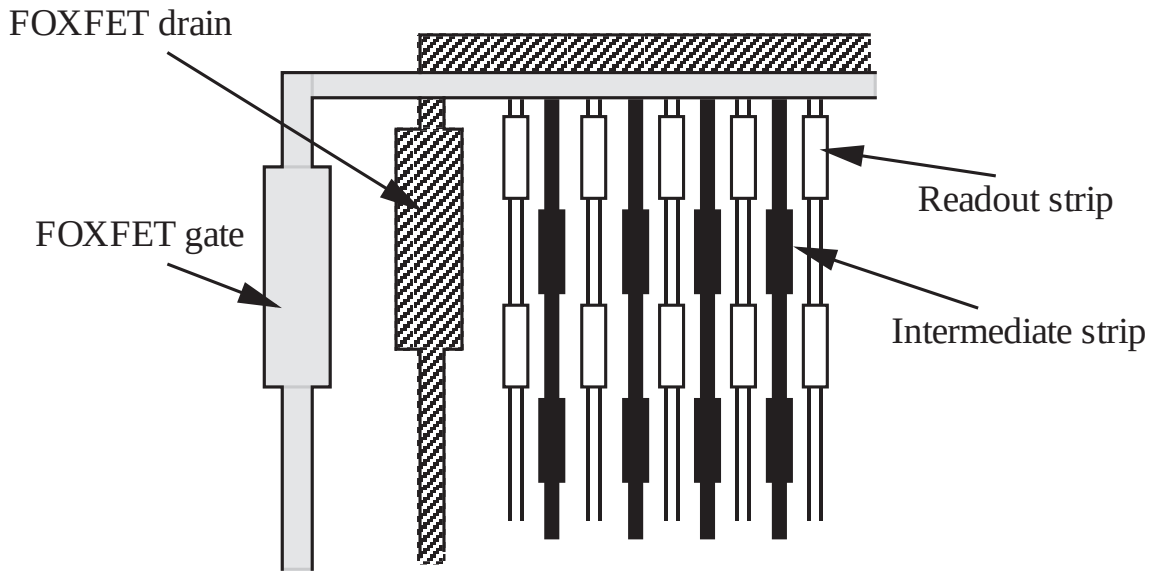

Figure 2: Schematic top view of a corner of a silicon sensor.

4 The off-line analysis

For its first operation, the telescope has been put on a 100 GeV pion beam at CERN. The z positions of the detectors were 2.4, 9.2, 212.4 and 219.2 mm for x measuring sensors and 0, 11.6, 210 and 221.6 mm for y measuring ones.

The pedestals and the common mode shift (common noise pickup on all channels) are subtracted from the raw data and the physical noise is estimated for each channel by using numerical filtering methods [9]. The noisy, saturated or dead channels have been rejected from all the analysis steps by appropriate cuts.

A standard method is then applied to select clusters, for each event and in each detector [9][10]. First, one looks for a strip with a signal over noise ratio $(\mathrm{S/N})_{strip} > \mathrm{T}_1$. Then all the neighbouring strips with $(\mathrm{S/N})_{strip} > \mathrm{T}_2$ are added to form a cluster. The cluster is accepted if $(\mathrm{S/N})_{cluster} > \mathrm{T}_3$ and if the number of strips in the cluster is less or equal to T_4.

The T_3 cut corresponds to the half of the most probable energy deposition of a MIP in the sensors. The low noise level allowed us to use severe values for T_1 and T_2 cuts. They have been defined by looking at the signal distribution for the central strip and for neighbouring ones. T_2 and T_4 cuts are correlated. To avoid redundancy, a very soft cut on the number of strips per cluster has been applied. The cuts are listed for

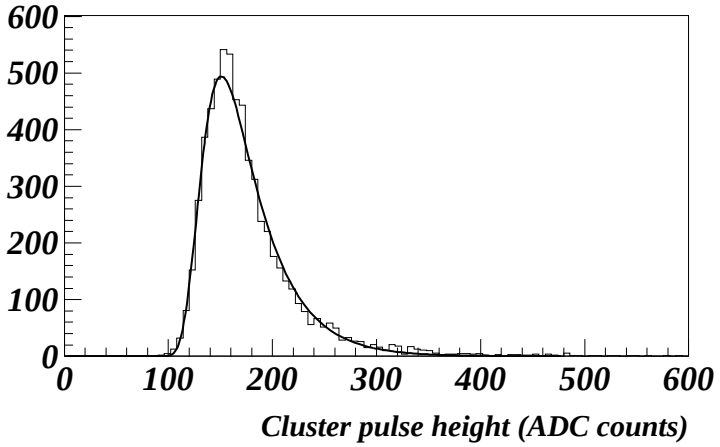

Figure 3: Pulse height distribution fitted by a Landau curve.

each detector in table 1 (The detector designations are the same as in figure 1).

T_i	X1	X2	X3	X4	Y1	Y2	Y3	Y4
T_1	20	20	20	15	20	20	20	15
T_2	3	3	3	2	3	3	3	2
T_3	53	54	58	29	37	52	53	42
T_4	15	15	15	15	15	15	15	15

table 1. T_i cut values for each detector.

Figure 3 shows the charge distribution measured by a typical detector. The most probable energy deposition corresponds to 156 ADC counts, while the noise mean value of this detector is 1.47 per strip, with a negligible error. A signal over noise ratio of 106 is thus obtained.

For hit position computation and resolution analysis, a zero value has been used for T_2 in order to avoid single strip clusters. Hit position in the clusters are computed by using the ETA algorithm [11] [12], since the detectors are perpendicular to the beam. It consists of a non linear interpolation between the two neighbouring strips of the cluster which have collected the highest signals. The hit position, in pitch unit, between these two strips is given by :

$$X_0 = \frac{1}{N_t} \int_0^{\eta_0} \frac{dN}{d\eta} d\eta \qquad (1)$$

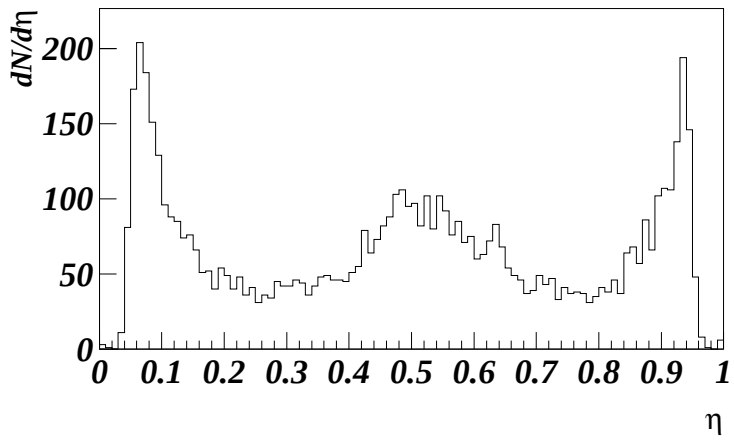

Figure 4: $\frac{dN}{d\eta}$ distribution.

where N_t is the total number of entries in the $\frac{dN}{d\eta}$ distribution and η_0 is the fraction of the signal collected by the left strip, in the considered event. η is given by :

$$\eta = \frac{S_L}{S_L + S_R} \tag{2}$$

The $\frac{dN}{d\eta}$ distribution is shown for one detector in figure 4. The 3 peak structure is typical for two neighbouring readout strips separated by a non-read one [12][13].

5 Results

Tracks are reconstructed with a least square fit based on the hit positions in the 2x4 detectors. Only tracks with a hit in all the detectors and with a slope less than 2 $mrad$ in both views (x and y) are used for the alignement. The worst observed misalignement was a 14 $mrad$ tilt in the detector plane of one single sensor.

After alignement corrections, redundancy was used to compute the efficiency of all individual detectors. A track is considered as detected if there is at least one strip in the vicinity of the extrapolated track in the detector under study such that:

- **i)** Its noise, and the individual noises of its six closest neighbours are lower than three times the average noise of all strips of the detector.

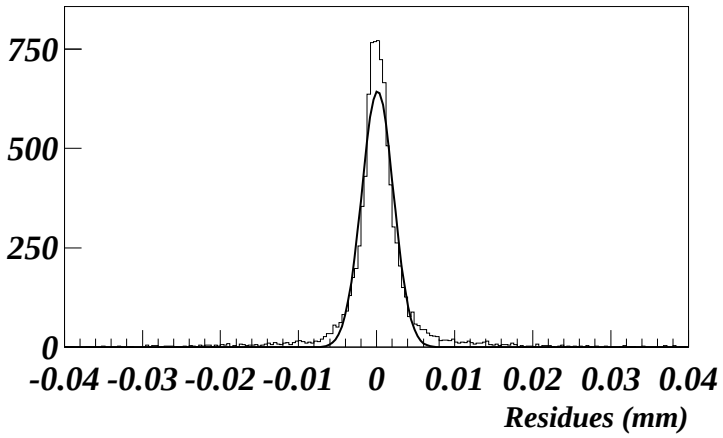

Figure 5: Residue distribution.

- **ii)** Its signal is larger than 10 times its noise.

Individual efficiencies are shown in table 2. The statistical uncertainties on these effeciencies are of the order of 0.1 %. The efficiency in the detector Y3 is low, due to 6 noisy strips, while there are 2 noisy strips in detector Y2. The inefficiency of these two detectors is due to the severity of the cuts. The efficiency loss can be recovered by narrowing the window around the central strip in condition **i)**. The main contribution to the inefficiencies in the other detectors comes from noise fluctuations. Asking for at least 3 planes with a hit in each view, the telescope efficiency was found to be 98.7 %.

	X1	X2	X3	X4	Y1	Y2	Y3	Y4
ϵ (%)	97.3	98.8	98.5	98.8	98.9	95.5	84.3	98.6
$\sigma(\mu m)$	1.5	1.5	1.4	1.6	1.3	1.3	1.3	1.3

table 2. Individual efficiencies and resolutions.

The residue distribution for a single detector is shown in figure 5. It is computed after removing the detector under study from the track fit. The intrinsic resolution of a detector is obtained by subtracting quadratically the extrapolation error (obtained analytically) from the standard deviation of the gaussian fit of the residue distribution. The multiple scattering contribution to this error [14] was found to be very small and thus neglected. Individual resolutions ranging from 1.3 to 1.6 μm were obtained (table

2). These results imply an extrapolation error in the middle of the telescope of 0.7 μm in each view for high momentum particles.

The obviously non-gaussian shape of the residues originates from two well known effects :

- **i)** High energy electrons from primary ionisation [15]: Such electrons displace the cluster position and spoil the resolution. Figure 6 shows the detector resolution as a function of the pulse height. One sees clearly the effect of high energy deposition in the detector.

- **ii)** The hit position between two readout strips [12][13]: It can be shown from equation (1) that the resolution is proportional to $\frac{dN}{d\eta}$. Figure 7 shows that the resolution has the same η dependence than $\frac{dN}{d\eta}$ (figure 4).

The $\frac{dN}{d\eta}$ and the signal over noise (S/N) distributions have been divided into 5 and 7 intervals respectively, leading us to 35 (η, S/N) cells, and to a 5x7 resolution matrix, for each detector. For each cell (i,j) and for each detector k, we have calculated the resolution σ_{ij}^k and the probability to have a hit in this cell P_{ij}^k, wich is the number of entries in the considered cell, divided by the total number of events seen by the detector k. The extrapolation error in the middle of the telescope, and its probability have been computed for each of the 35^4 combinations in each view. The result is shown in figure 8 wich represents the probability distribution of the extrapolation error in the x view, using the four detectors. The mean value of this distribution is 0.7 μm, in agreement with the value quoted above. The structures around 4 μm came from the high energy loss cells. To avoid such isolated structures, one needs a tighter subdivision in the S/N distribution, and thus, more statistics.

We can see from figure 8 that the probability to obtain an extrapolation error of 1 μm or less is 89.7 %. This probability drops to 68.2, 72.3, 53.0 and 64.6 % if we remove respectively either one of the four detectors. The probability distribution with 3 planes (in this case X4 removed) is shown in figure 9. It has been checked for this distribution that the accumulation of events at $\sigma_e = 6$ to $7\mu m$ comes uniquely from events where detector X3, or both X1 and X2 have a very high pulse height.

6 Conclusion

A compact and precise silicon telescope for beam test purposes has been built. It consists of 4 pairs of silicon sensors, with an average resolution of 1.4 μm per sensor. It is able to give a point position with a precision of 0.7 μm in both x and y coordinates, and with an efficiency of 98.7 %. It can be a powerfull tool to test not only high

precision tracking devices, but also conventional tracking detectors and calorimeter prototypes.

Acknowledgments

This work could not be achieved without the participation of our LEPSI and CERN technicians and engineers. We would like to express our gratitude to R. Boulter, R. Fischer, C. Illinger, N. Mayet, R. Osswald, R. Priss and K. Ratz.

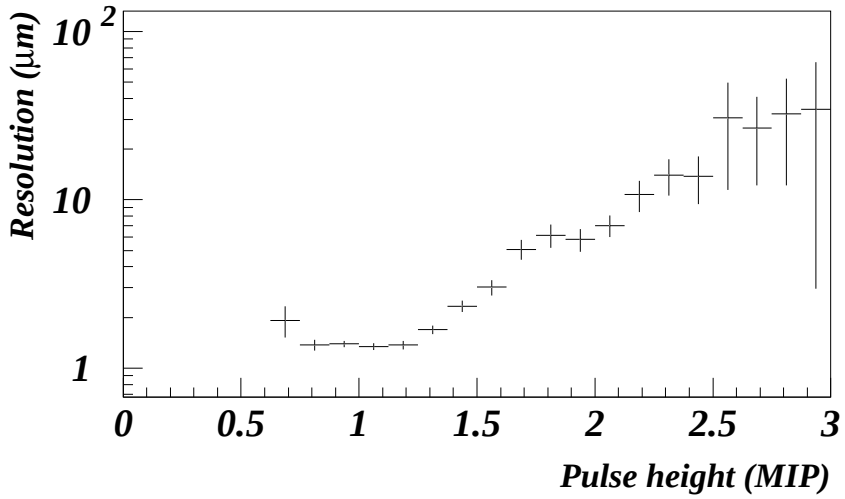

Figure 6: Pulse height dependance of the resolution.

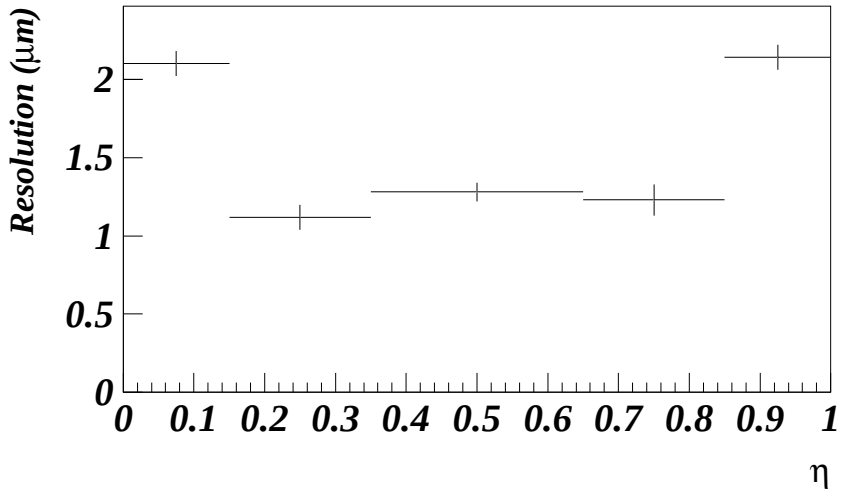

Figure 7: η dependence of the resolution.

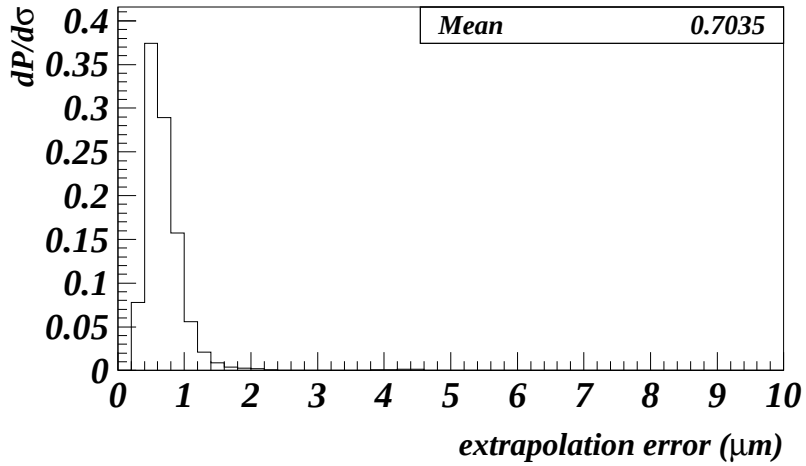

Figure 8: Probability density distribution of the extrapolation error in the middle of the telescope, with the four X sensors.

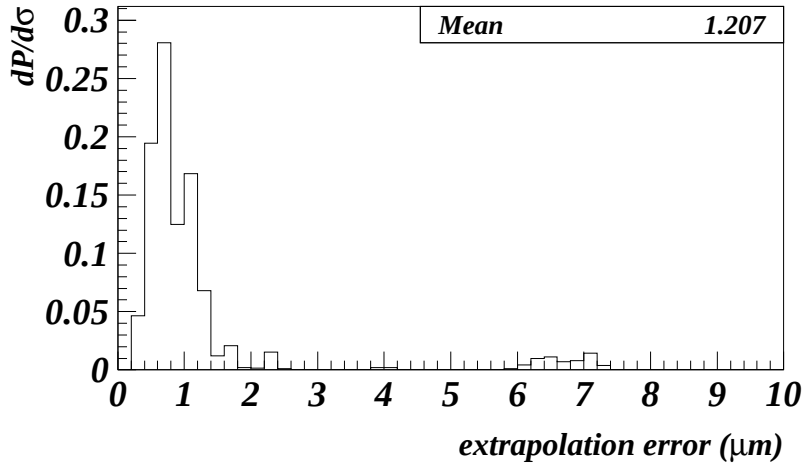

Figure 9: Probability density distribution of the extrapolation error with three sensors (X4 removed).

References

[1] P. Weilhammer, Nucl. Instr. and Meth. A342 (1994) 1.

[2] E. Heijne et al., Nucl. Instr. and Meth. A273 (1988) 615 and P. Delpierre et al. (RD 19 collaboration), Nucl. Instr. and Meth. A342 (1994) 233.

[3] F. Borchet et al., CERN PPE/94-113 and R&D Proposal, CERN/DRDC 94-21, DRDC/P56 (RD 42 collaboration).

[4] A. Oed, Nucl. Instr. and Meth. A263 (1988) 351 and R&D Proposal, CERN/DRDC 92-30, DRDC/P41 (RD 28 collaboration).

[5] S. P. Beaumont et al. (RD 8 collaboration), Nucl. Instr. and Meth. A321 (1992) 172.

[6] O. Toker et al., Nucl. Instr. and Meth. A340 (1994) 572.

[7] N. Bingefors et al., CERN/PRE 88-088.

[8] A. Bogaerts, CERN DD Division, Microdas manual, DD/OC/ND, 1985, unpublished.

[9] V. Chabaud et al., Nucl. Instr. and Meth. A292 (1990) 75.

[10] L. Hubbeling et al., Nucl. Instr. and Meth. A310 (1991) 197.

[11] E. Belau et al., Nucl. Instr. and Meth. 214 (1983) 253.

[12] R. Turchetta, Nucl. Instr. and Meth. A335 (1993) 44.

[13] A. Peisert, Instrumentation on High Energy Physics, F. Sauli editor, World Sci., Singapore 1992.

[14] G. Lutz, Nucl. Instr. and Meth. A273 (1988) 349.

[15] P. Weilhammer, Proceedings of the Workshop on New Solide State Devices for High Energy Physics, Berkeley, 1987.